MRS Advances (2022) 7:128–133
https://doi.org/10.1557/s43580-022-00226-1

ORIGINAL PAPER

Structural incorporation of lanthanides (La, Eu, and Lu) into U_3O_8 as a function of the ionic radius

Shannon Kimberly Potts[1] · Philip Kegler[1] · Giuseppe Modolo[1] · Simon Hammerich[2] · Irmgard Niemeyer[1] · Dirk Bosbach[1] · Stefan Neumeier[1]

Received: 22 November 2021 / Accepted: 31 January 2022 / Published online: 9 February 2022

Abstract

The International Atomic Energy Agency implements safeguard measures to verify the compliance of Member States to their international legal obligations using nuclear material and technology only for peaceful purposes. These safeguard measures, *i.a.*, include analytical measurements of individual micrometer- and submicrometer particles taken by the IAEA on swipe samples during safeguard inspections at nuclear facilities. To ensure the quality control of the analytical results from particle analysis and to further develop mass spectrometric analysis methods, microparticles with well-defined properties as microparticulate reference materials are required. Therefore, mixed lanthanide/uranium oxide microparticles were produced as a first step towards composite reference materials with small amounts of fission products, Pu or Th. A deep understanding of the incorporation mechanisms of dopants into U_3O_8 structure is essential in this regard. Therefore, bulk-scale comparison materials were produced and doped with lanthanides by co-precipitation methods and systematically investigated by TG, XRD, and Raman. These results will be integrated into the particle production process to design well-defined microparticulate mixed-oxide reference materials.

Introduction

The International Atomic Energy Agency (IAEA) expressed a significant demand on nuclear reference materials in order to sustain a robust quality control (QC) system. This QC system includes instrument calibration as well as method development and proficiency testing [1]. Such nuclear reference materials are used by the IAEA's Office of Safeguards Analytical Services (IAEA-SGAS) and their worldwide Network of Analytical Laboratories (NWAL) [2]. These materials must fulfill certain requirements, such as well-designed micrometer and submicrometer-sized reference microparticles with precisely defined elemental and isotopic composition, size, and morphology to ensure the reliability of the mass spectrometric analytical measurements [1]. For this propose, a physical aerosol-based approach was established and implemented in the safeguards laboratory at Forschungszentrum Jülich leading to certified microparticulate reference materials [2–5]. The advanced development of mass spectrometric analytical methods such as Large Geometry–Secondary Ion Mass Spectrometry (LG-SIMS) and Thermal Ionization Mass Spectrometry (TIMS) with regard to the increas in the sensitivity (detection limit) and selectivity for the detection of even small amounts of fission products goes hand in hand with the optimization of existing and development of new reference materials [2, 3, 6–8]. Pure uranium and composite (U-lanthanides (*Ln*'s), U–Th and U–Pu) reference materials in microparticulate form are of particular interest in this context. As a result, neodymium-doped uranium oxide microparticles were successfully synthesized and characterized via Scanning Electron Microscopy (SEM) and Energy-Dispersive X-ray Spectroscopy (EDS) [9]. However, this aerosol-based method at the Forschungszentrum Jülich is limited in its yield (µg range) and hence leads to certain analytical challenges, particularly in view of investigations on the chemical behavior and consecutively on the stability. Therefore, internal reference materials with various *Ln*'s on bulk scale were synthesized and characterized to investigate the structural incorporation

✉ Shannon Kimberly Potts
s.potts@fz-juelich.de

[1] Forschungszentrum Jülich GmbH, Institute of Energy and Climate Research – Nuclear Waste Management and Reactor Safety (IEK-6), 52425 Jülich, Germany

[2] Heidelberg University, Institute of Earth Sciences, 69120 Heidelberg, Germany

of the dopants into the U_3O_8 structure to transfer these findings to the *3D* confined microparticulate system.

This work represents recent results on the preparation of *Ln*-doped U_3O_8 materials as the first step towards *Ln*-doped as well as Th- and Pu-doped microparticulate reference materials for analytical measurements in nuclear safeguards.

Materials and methods

Within this work no experiments on human and animal subjects are reported.

Synthesis of the doped and undoped ammonium diuranate, $(NH_4)_2U_2O_7$

The bulk-scale comparison materials were produced via co-precipitation adapted from Kegler et al. [10]. Aqueous $UO_2(NO_3)_2{\cdot}6\ H_2O$ (p.A., Merck KGaA) solutions containing-10 mol% *Ln*-nitrate (c(metal) = 2 mol·L^{-1}) with the *Ln*-compounds $La(NO_3)_3{\cdot}6\ H_2O$ (99.99%, Sigma Aldrich), $Eu(NO_3)_3{\cdot}6\ H_2O$ (99.99%, Alfa Aesar), and $Lu(NO_3)_3{\cdot}x\ H_2O$ (99.99%, Alfa Aesar) were prepared. Ammonia ($w(NH_3)$ = 32%; Merck KGaA) was used as the precipitant in this synthesis with an excess of at least 300% to shift the equilibrium to the product side. These mixed uranyl/*Ln*-nitrate solutions were slowly added to ammonia while stirring. For quantitative precipitation the mixture was then stirred for two hours. The synthesized doped and undoped ammonium diuranate (ADU) materials were washed several times with MilliQ® water (18.2 MΩ resistivity, Elga PURELAB Ultra installation) and centrifuged using a HERAEUS Multifuge 3SR + and finally elutriated with ethanol (p.A., Merck KGaA) and dried at room temperature [10].

Characterization of the bulk-scale comparison materials

The thermally induced phase formation of the synthesized materials was analyzed via thermogravimetric analyses (TG) measurements using a *NETZSCH* STA 449 F1 Jupiter. The measurements were carried out in Pt/Rh crucibles with heating rate of 10 K·min^{-1} in synthetic air (80/20).

The doped and undoped materials were calcined at 520 °C and 700 °C in air using the CARBOLITE CWF 1300 chamber furnace. The chemical composition of the La-, Eu-, and Lu-doped materials after calcination at 700 °C was confirmed by using a FEI Quanta 200F environment scanning electron microscope equipped with an energy-dispersive X-ray spectrometer operated in low vacuum modus (60 Pa) at 20 kV. The abundance of 14.(4) at% La, 16.(4) at% Eu, and 13.(4) at% Lu were determined in the doped materials using EDS. The deviation of these results from the theoretical doping level of 10 mol% is in error margin of the device as well as of the initial weight.

X-ray Diffraction (XRD) patterns of the materials after calcination were recorded by means of a Bruker D4 Endeavor diffractometer equipped with a *1D* Lynx-eye detector in Bragg–Brentano configuration using $CuK_{\alpha1,2}$ radiation (λ = 1.54184 Å). XRD data were collected at room temperature in the $10° \leq 2\theta \leq 120°$ range with a step size of $(2\theta) = 0.01°$ and a counting time of 2 s per step, leading to a total counting time of about 6 h. Lattice parameters were refined by the Rietveld method using GSAS2 software [11]. A pseudo-Voigt function was used for lattice parameter refinement.

The Raman spectra of the obtained undoped and La-, Eu-, and Lu-doped U_3O_8 were collected using a Horiba LabRAM HR spectrometer with a Peltier-cooled multichannel CCD detector. Therefore, small quantities of the synthesized powder had to be pressed into pellets. The Raman spectra of the compounds were recorded at room temperature in the range of 100 cm^{-1} to 1000 cm^{-1} using a He–Ne laser at a power of 17 mW (λ = 632.81 nm). The spectral resolution was around 1 cm^{-1} with a slit of 100 µm.

Results and discussion

The bulk-scale comparison materials synthesized via co-precipitation method, which are initially available as ADU, were systematically investigated to understand the mechanism of structural incorporation of different *Ln*'s into U_3O_8 structure as a function of ionic radius. A doping level of 10 mol% *Ln* (*Ln* = La, Eu, and Lu) was selected enabling the detection of incorporation or phase segregation with state-of-the-art analytical methods. The information obtained from these investigations allows for drawing first conclusions regarding the formation of single phases or phase segregations induced by the dopant and consequently also regarding the stability of the mixed-oxide microparticles. TG measurements were carried out in order to understand the decomposition of the undoped and doped ADU as well as the temperature ranges of the phase transitions. Figure 1 (left) represents the mass loss as a function of the calcination temperature of the undoped ADU. The first significant recorded mass loss up to a temperature of 500 °C corresponds to the removal of H_2O and NH_3 and the formation of UO_3. This decomposition is in accordance with the observations in the literature [12, 13]. The next mass loss step can be assigned to the conversion of UO_3 to U_3O_8. This phase transition takes place in a temperature range of 520 °C to 700 °C. Similar results were observed for the 10 mol% La-, Eu-, and Lu-doped materials (see Fig. 1, enclosed zoom) with a clear dependence of the dopants' ionic radii. The temperature range of the phase

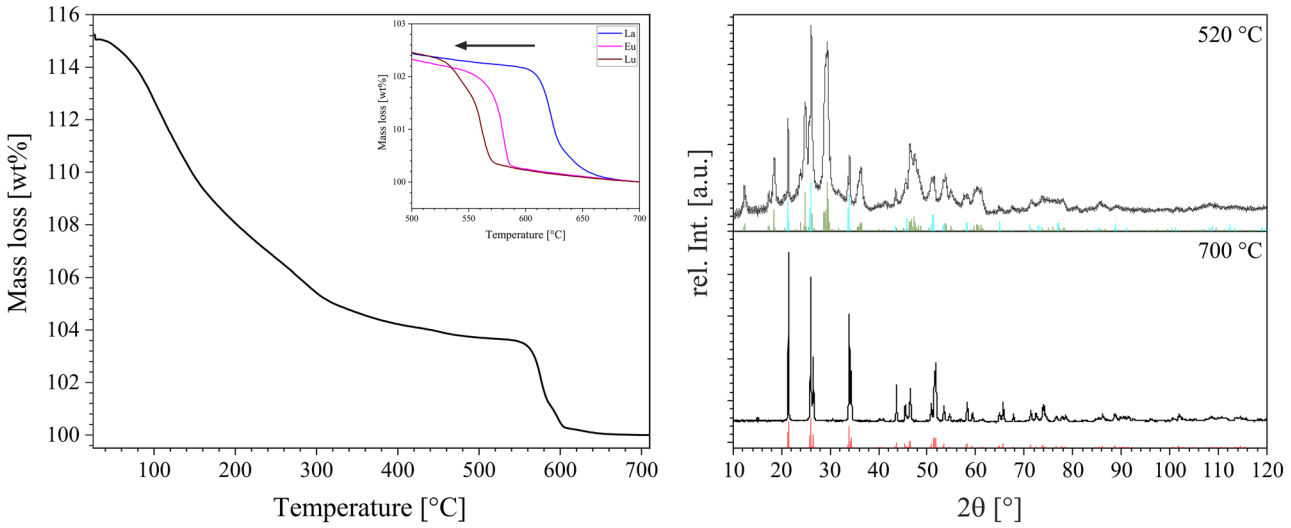

Fig. 1 Left: Thermogram of the undoped ADU, including an enclosed zoom of the TG measurements in the temperature range from 500 °C to 700 °C of the materials doped with 10 mol% La (blue), Eu (magenta), and Lu (brown) measured in synthetic air, masses normalized to $m(U_3O_8)$ at 700 °C. Right: X-ray diffractograms of the undoped materials after calcination at 520 °C (top) (References: α-UO_3 with the space group *C2mm* (cyan) [14]; β-UO_3 with the space group $P2_1$ (dark green) [13]) and 700 °C (bottom) (Reference: U_3O_8 with the space group *C2mm* (red) [15])

transition from UO_3 to U_3O_8 is shifted to lower temperature ranges with the decrease in ionic radii of the dopants (cf. Table 1) indicating the influence of the ionic radius of the dopants on the phase transformation from UO_3 to U_3O_8.

In order to identify the phases in these temperature limits precisely, XRD measurements on the undoped material were carried out after calcination at 520 °C and 700 °C (Fig. 1, right). The XRD pattern shows the formation of a phase mixture of α-UO_3 and β-UO_3 after calcination at 520 °C and of a pure orthorhombic α-U_3O_8 phase with the space group *C2mm* after calcination at 700 °C, which is stable at room temperature [15]. Both the formation of the phase mixture of α-UO_3 and β-UO_3 and the formation of orthorhombic U_3O_8 were to be expected for the undoped material in this temperature range and correspond to the literature [13, 16, 17].

Since the microparticles produced at Forschungszentrum Jülich crystallize despite the low calcination temperature of 500 °C in the orthorhombic U_3O_8 phase [2, 3], the focus of this work is set on the investigation of the U_3O_8 phase formation as a function of the ionic radius of the dopant. Based on the results derived from TG and XRD measurements, the formation of the U_3O_8 phase occurs after calcination at 700 °C. The discussion of following results is therefore only related to the La-, Eu-, and Lu-doped bulk-scale comparison materials which were calcined at 700 °C.

Figure 2 depicts the measured X-ray diffractograms of the various *Ln*-doped materials after calcination. The XRD pattern suggests phase pure compounds similar to the α-U_3O_8 phase. No additional reflex was identified pointing to the formation of any other *Ln*-rich phase, e.g., Ln_2O_3. A distinct deviation from the XRD pattern of the orthorhombic α-U_3O_8 phase can be observed on the reflex positions around 26° and 34° (see Fig. 2, enclosed zoom). While the undoped material has two significant reflexes at both reflection positions, these are merged into single reflexes for the doped materials. Such a diffraction pattern corresponds to the formation of a hexagonal metastable α'-U_3O_8 phase with the space group $P\bar{6}2m$. According to Ackermann et al. [15], the pure orthorhombic U_3O_8 phase transforms into hexagonal α'-U_3O_8 phase at temperatures above 350 °C. This leads to the conclusion that the Ln^{3+} doping of the U_3O_8 results in a structural transformation from the space group *C2mm*

Table 1 Fit parameters obtained from Rietveld refinement and lattice volume calculated for the pure U_3O_8 and for 10 mol% La-, Eu-, and Lu-doped hexagonal U_3O_8

Sample	Ionic radius of *Ln* [18] [Å]	Lattice volume [Å^3]	Normalized volume [Å^3]	GOF [%]	wR_p [%]
La-doped U_3O_8 ($P\bar{6}2m$)	1.172	168.76(5)	337.52(5)	4.42	7.760
Eu-doped U_3O_8 ($P\bar{6}2m$)	1.087	167.35(6)	334.70(6)	4.80	9.077
Lu-doped U_3O_8 ($P\bar{6}2m$)	1.001	165.21(6)	330.42(6)	4.21	7.621
Pure U_3O_8 (*C2mm*)	/	333.08(1)	333.08(1)	4.30	8.385

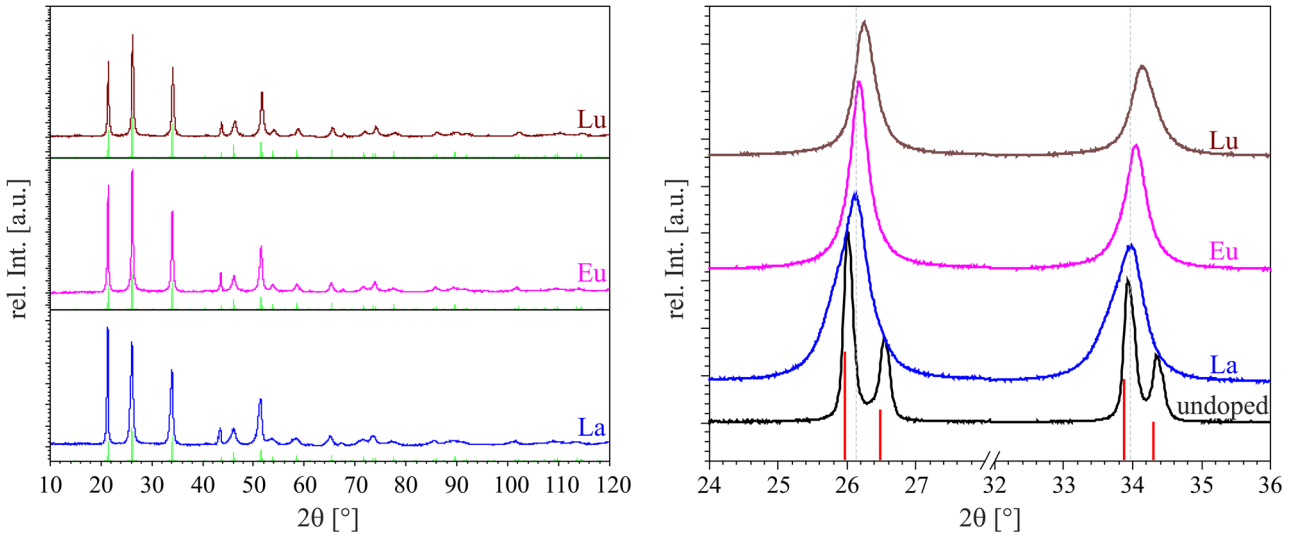

Fig. 2 X-ray diffractograms of the calcined materials (left) doped with 10 mol% La (blue), Eu (magenta), and Lu (brown), including zoom of the X-ray diffractograms (right) in the 2θ range from 24° to 36° (References: U_3O_8 with the space group $P\bar{6}2m$ (green) [20]; U_3O_8 with the space group $C2mm$ (red) [15])

to $P\bar{6}2m$ as well as to the stabilization of the metastable α'-U_3O_8 phase at room temperature. A similar observation is described in the literature for the doping of U_3O_8 with 10 mol% Am [19].

The zoom in Fig. 2 additionally shows a shift in the reflex positions depending on the ionic radii of *Ln* according to the Vegard's law. Rietveld refinements were carried out for the doped hexagonal U_3O_8 materials as well as for the pure orthorhombic U_3O_8. The determined unit cell volumes of the doped U_3O_8 materials with space group $P\bar{6}2m$ (see Table 1) are for La 168.76(5) Å^3, Eu 167.35(6) Å^3, and Lu 165.21(6) Å^3. These total lattice volumes correspond to the volume contraction for the unit cell for the *Ln*-doped hexagonal U_3O_8 as a function of the ionic radii (Table 1). Refinement of the pure orthorhombic U_3O_8 resulted in a total lattice volume of 333.08(1) Å^3. Comparing the now normalized volume of each crystalline structure (Table 1) with pure U_3O_8, the La- and Eu-containing samples clearly show a lattice expansion of the structure. The global increase is between a range of 4.44 Å^3 (La) and 1.62 Å^3 (Eu), which is a significant value range for the lattice modification and supports the hypothesis of the La and Eu substitution at a U-site in the U_3O_8. Caisso et al. [19] also reported such a volume expansion due to the structural incorporation of Am into the hexagonal U_3O_8 phase. However, this swelling cannot be detected for the Lu-doped U_3O_8. This deviation indicates that Lu, due to the smaller ionic radius compared to La and Eu, occupies U-sites that apparently leads to a volume contraction, most probably since the ionic radius of Lu is roughly in the range of uranium ($r(U^{6+})=0.87$ Å; $r(U^{5+})=0.9$ Å) [16].

Due to the asymmetrical shape of the reflexes in the X-ray diffractogram of the La-doped material (see Fig. 1, enclosed zoom), the formation of a pure hexagonal U_3O_8 phase can be excluded, but rather the presence of an orthorhombic U_3O_8 phase fraction in the material can be assumed. It can be concluded that La^{3+} cannot be incorporated homogenously into the hexagonal phase due to large ionic radius. This could in turn lead to a phase separation from a hexagonal phase system during calcination to a mixture of orthorhombic and hexagonal U_3O_8, while the material cools down to room temperature.

Raman measurements were then performed to verify the absence of additional segregated *Ln*-rich phases, which was not detected by XRD, and to identify short-range order phenomena of the phases for the doped and undoped materials (Fig. 3). Exclusively vibrations of the U_3O_8 phase could be identified in the Raman spectra (see Supplementary information, Table A1) [21, 22]. The exact assignment of the vibrations is given in the supporting information. The absence of vibration modes of the compounds La_2O_3 [23, 24], Eu_2O_3 [25, 26], and Lu_2O_3 [26–28] in the Raman spectra of the doped materials confirms the structural incorporation of *Ln*'s into U_3O_8. The results from TG, XRD as well as the Raman measurements thus indicate that the dopants are quantitatively incorporated into the U_3O_8 structure.

Conclusion

The incorporation of *Ln*'s (La, Eu, Lu) into the orthorhombic U_3O_8 crystal structure was investigated as a function of ionic radius at 700 °C. All *Ln*'s are accommodated by

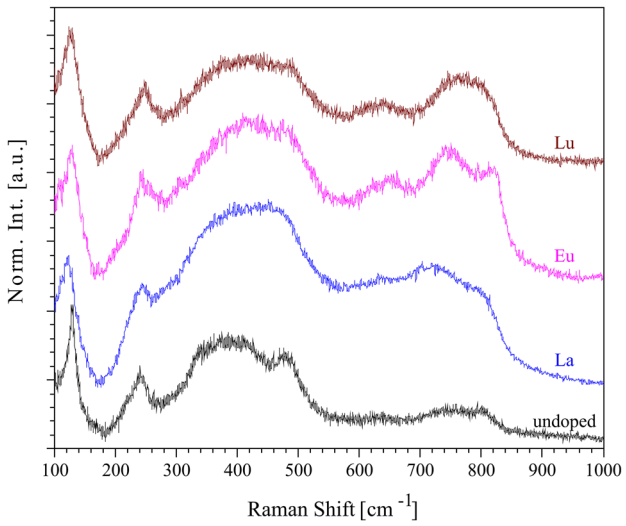

Fig. 3 Raman spectra of pure U_3O_8 (black) and U_3O_8 doped with 10 mol% La (blue), Eu (magenta), and Lu (brown)

U_3O_8 combined with a phase transition from orthorhombic to hexagonal U_3O_8 structure. However, for the largest *Ln*, La, the phase transition to hexagonal structure was not quantitatively completed most probably due to a size effect of the ionic radius. These results clearly demonstrate the feasibility to produce homogeneous phase of pure doped U_3O_8 microparticles. The incorporation can be expected to occur at lower temperature for the microparticles due to *3D* confinement and improved thermal convection in micro-sized materials.

Supplementary Information The online version contains supplementary material available at https://doi.org/10.1557/s43580-022-00226-1.

Acknowledgments This publication was prepared as an account of work within the Joint Programme on the Technical Development and Further Improvement of IAEA Safeguards between the Federal Republic of Germany and the IAEA. The work was funded by the Federal Ministry for Economic Affairs and Energy, Germany under Task C45/A1961. We acknowledge N. Lieck from Forschungszentrum Jülich GmbH for experimental and analytical support. The datasets generated during and/or analyzed during the current study are available from the corresponding author on reasonable request.

Funding Open Access funding enabled and organized by Projekt DEAL.

Declarations

Conflict of interest On behalf of all authors, the corresponding author states that there is no conflict of interest.

References

1. K.G.W. Inn, C.M. Johnson, W. Oldham, S. Jerome, L. Tandon, T. Schaaff, R. Jones, D. Mackney, P. MacKill, B. Palmer, D. Smith, S. LaMont, J. Griggs, J. Radioanal. Nucl. Chem. **296**, 5–22 (2012)
2. S. Neumeier, R. Middendorp, A. Knott, M. Dürr, M. Klinkenberg, F. Pointurier, D.F. Sanchez, V.-A. Samson, D. Grolimund, I. Niemeyer, D. Bosbach, MRS Adv. **3**, 1005–1012 (2018)
3. R. Middendorp, M. Durr, A. Knott, F. Pointurier, D. Ferreira-Sanchez, V. Samson, D. Grolimund, Anal. Chem. **89**, 4721–4728 (2017)
4. J. Truyens, M. Dürr, Z. Macsik, R. Middendorp, S. Neumeier, S. Richter, G. Stadelmann, C. Venchiarutti, Y. Aregbe, *EUR29840* (Publications Office of the European Union, Luxembourg, 2020)
5. J. Truyens, S. Neumeier, P. Kegler, M. Klinkenberg, M. Zoriy, S. Richter, Y. Aregbe, *EUR30625* (Publications Office of the European Union, Luxembourg, 2021)
6. R. Middendorp, M. Klinkenberg, M. Dürr, J. Radioanal. Nucl. Chem. **318**, 907–914 (2018)
7. S. Boulyga, S. Konegger-Kappel, S. Richter, L. Sangély, J. Anal. At. Spectrom. **30**, 1469–1489 (2015)
8. Y. Ranebo, P.M.L. Hedberg, M.J. Whitehouse, K. Ingeneri, S. Littmann, J. Anal. At. Spectrom. **24**, 277–287 (2009)
9. P. Kegler, F. Pointurier, J. Rothe, K. Dardenne, T. Vitova, A. Beck, S. Hammerich, S. Potts, A.-L. Faure, M. Klinkenberg, MRS Adv. **6**, 125–130 (2021)
10. P. Kegler, M. Klinkenberg, A. Bukaemskiy, G.L. Murphy, G. Deissmann, F. Brandt, D. Bosbach, Materials **14**, 6160 (2021)
11. B.H. Toby, J. Appl. Crystallogr. **34**, 210–213 (2001)
12. C. Schreinemachers, G. Leinders, G. Modolo, M. Verwerft, K. Binnemans, T. Cardinaels, Nucl. Eng. Technol. **52**, 1013–1021 (2020)
13. P. Debets, Acta Cryst. **21**, 589–593 (1966)
14. B.O. Loopstra, E.H.P. Cordfunke, Recl. Trav. Chim. Pays-Bas **85**, 135–142 (1966)
15. R. Ackermann, A. Chang, C.A. Sorrell, J. Inorg. Nucl. Chem. **39**, 75–85 (1977)
16. N.B.A. Thompson, V.L. Frankland, J.W.G. Bright, D. Read, M.R. Gilbert, M.C. Stennett, N.C. Hyatt, J. Radioanal. Nucl. Chem. **327**, 1335–1347 (2021)
17. X. Guo, D. Wu, H. Xu, P.C. Burns, A. Navrotsky, J. Nucl. Mater. **478**, 158–163 (2016)
18. R.D. Shannon, Acta Cryst. **A32**, 751–767 (1976)
19. M. Caisso, P. Roussel, C. Den Auwer, S. Picart, C. Hennig, A.C. Scheinost, T. Delahaye, A. Ayral, Inorg. Chem. **55**, 10438–10444 (2016)
20. B. Loopstra, J. Appl. Crystallogr. **3**, 94–96 (1970)
21. I.S. Butler, G.C. Allen, N.A. Tuan, Appl. Spectrosc. **42**, 901–902 (1988)
22. S.D. Senanayake, R. Rousseau, D. Colegrave, H. Idriss, J. Nucl. Mater. **342**, 179–187 (2005)
23. J. Cui, G.A. Hope, J. Spectrosc. **2015**, 940172 (2015)
24. J. Denning, S. Ross, J. Phys. C: Solid State Phys. **5**, 1123–1133 (1972)
25. M.W. Urban, B.C. Cornilsen, J. Phys. Chem. Solids **48**, 475–479 (1987)

26. M.V. Abrashev, N.D. Todorov, J. Geshev, Int. J. Appl. Phys. **116**, 103508 (2014)
27. A. Garcıa-Murillo, C. Le Luyer, C. Pedrini, J. Mugnier, J. Alloys Compd. **323**, 74–77 (2001)
28. L. Laversenne, Y. Guyot, C. Goutaudier, M.T. Cohen-Adad, G. Boulon, Opt. Mater. **16**, 475–483 (2001)